Published in final edited form as:
Nanoscale. 2010 July 7; 2(7): 1141–1148. doi:10.1039/c0nr00102c.

Multifunctional nanocomposites of superparamagnetic (Fe_3O_4) and NIR-responsive rare earth-doped up-conversion fluorescent ($NaYF_4$: Yb,Er) nanoparticles and their applications in biolabeling and fluorescent imaging of cancer cells

Congcong Mi[a], **Jingpu Zhang**[a], **Huanyu Gao**[a], **Xianlong Wu**[a], **Meng Wang**[a], **Yingfan Wu**[c], **Yueqin Di**[c], **Zhangrun Xu**[c], **Chuanbin Mao**[*,b], and **Shukun Xu**[*,a]

[a]Department of Chemistry, Northeastern University, Shenyang, 110004, P. R. China.

[b]Department of Chemistry & Biochemistry, University of Oklahoma, 620 Parrington Oval, Room 208, Norman, OK, 73019, USA.

[c]Research Center for Analytical Sciences, Northeastern University, Shenyang, 110004, P. R. China

Abstract

A new kind of magnetic/luminescent multifunctional nanoparticles was synthesized by covalently linking multiple carboxyl-functionalized superparamagnetic Fe_3O_4 nanoparticles and individual amino-functionalized silica-coated fluorescent $NaYF_4$: Yb,Er up-conversion nanoparticles (UCNPs). The resultant nanocomposites bear active carboxylic and amino groups on the surface that were proved to be chemically active and useful for further facile bioconjugation with biomolecules. The UCNPs in the nanocomposite particles can emit visible light in response to the irradiation by near infrared (NIR) light, enabling the application of the nanocomposites in bioimaging. X-Ray diffraction, infrared spectroscopy, transmission electron microscopy, luminescence spectroscopy, and magnetometry were applied to characterize the multifunctional nanocomposites. The nanocomposites exhibited good superparamagnetic and excellent green up-conversion photoluminescent properties that can be exploited in magnetic separation and guiding as well as bioimaging. Due to the presence of active functional groups on the nanocomposite surface, the Fe_3O_4/$NaYF_4$: Yb,Er magnetic/luminescent nanocomposites were successfully conjugated with a protein called transferrin, which specifically recognizes the transferrin receptors overexpressed on HeLa cells, and can be employed for biolabeling and fluorescent imaging of HeLa cells. Because NIR light can penetrate biological samples with good depth without damaging them and can avoid autofluorescence from them, the presence of both NIR-responsive UCNPs and superparamagnetic nanoparticles in the nanocomposite particles will enable the practical application of the nanocomposites in bioimaging and separation.

1. Introduction

In the past two decades, a great deal of work has been done to study superparamagnetic iron oxide nanoparticles (NPs) such as magnetite (Fe_3O_4) and maghemite (γ-Fe_2O_3).[1] Fe_3O_4 NPs are the most intensively studied magnetic nanoparticles and can be applied in a variety of areas, ranging from drug delivery and biosensing,[2] dynamic sealing[3] and cell labeling, to magnetic resonance imaging.[4,5] Recently, more attention was paid to the preparation of a

*xushukun46@126.com; Tel: +86 24 83681343, cbmao@ou.edu; Tel: +1 405 325 4385.

bifunctional nanostructure made of Fe_3O_4 and other NPs.[6–8] Since the incorporation of fluorescent dyes onto silica shells through covalent coupling,[9] efforts have been made to prepare a bifunctional nanocomposite of magnetic NPs and quantum dots (QDs).[10–12] For example, intracellular manipulation of fluorescent/magnetic CdSe/Fe_3O_4 NPs using a small magnet was recently demonstrated,[13] indicating it is possible for the nanocomposites to serve as a vehicle for the delivery of activators or inhibitors specifically to epithelial cells under a magnetic field. The QDs based magnetic/fluorescent composites were usually prepared by layer-by-layer and seeded growth methods.[14–16] The connection between the magnetic and fluorescent components in the resultant composites may not be very stable. A possible way to improve the stability of magnetic/fluorescent composite NPs is to covalently link magnetic and fluorescent components. We recently covalently linked multiple thioglycolic acid stabilized CdTe QDs with individual thiolfunctionalized silica-coated Fe_3O_4 to form nanocomposites through disulfide bonding.[17] The fluorescence intensity of the as-synthesized Fe_3O_4/CdTe magnetic/fluorescent nanocomposites was comparable to that of the pure CdTe QDs.

Synchronously, rare earth doped luminescent NPs were also integrated with magnetic NPs to prepare magnetic/luminescent composites.[18] For instance, spray pyrolysis was employed to synthesize Fe_3O_4/Eu : Gd_2O_3 core–shell NPs, which were further biofunctionalized with NeutrAvidin for the development of a rapid, simple and non-polymerase chain reaction based DNA hybridization-in-solution assay to quantify bacteria capable of biodegrading methyl tertiary-butyl ether.[19] A facile homogenous precipitation method[20] was later developed to synthesize multifunctional magnetic/luminescent nanocomposites using Fe_3O_4 NPs as the core and europium-doped yttrium oxide (Y_2O_3 : Eu) as the shell. These nanocomposites were functionalized with biotin which can specifically target avidin-coupled polystyrene beads. More recently, targeted cancer imaging was demonstrated by using doped oxide nanocrystals which show bright red-fluorescence and magnetic resonance imaging.[21] For this purpose, bifunctional magnetic/luminescent nanocomposites Fe_3O_4@-SiO_2/Y_2O_3 : Tb were formed by assembling Y_2O_3 : Tb nanorods onto the surface of Fe_3O_4@SiO_2 core–shell nanostructures.[22]

Up-conversion nanoparticles (UCNPs) can convert a longer wavelength radiation (*e.g.*, NIR light with 980 nm wavelength) to shorter wavelength fluorescence (*e.g.*, green visible light) *via* a two-photon or multi-photon mechanism.[23] They have properties desired for bioimaging such as high quantum yields, narrow emission peak, large Stokes shifts, good chemical stability, and low toxicity.[24] Because NIR light can be used to excite UCNPs, the use of UCNPs in bioimaging can minimize auto-fluorescence and result in improved signal-to-noise ratio and detection sensitivity.[25–27] Moreover, NIR light has higher penetration ability while being less harmful to cells.[28] As a result, UCNPs are considered better probes for cell imaging than conventional QDs in biological and clinical applications.[29,30] However, little work has been done to form a nanocomposite where magnetic NPs and UCNPs are integrated.[18] An attempt was made to synthesize NPs *via* covering Fe_3O_4 magnetic core with ytterbium and erbium co-doped sodium yttrium fluoride ($NaYF_4$: Yb,Er) as a shell.[31] The phosphor shell was prepared by co-precipitation of the rare-earth metal salts with fluoride in the presence of EDTA and the magnetic nanoparticle.

So far, there have been no reports on the covalent coupling of multiple Fe_3O_4 NPs with individual UCNPs such as $NaYF_4$: Yb,Er as the core and their applications in biolabeling of cancer cells. In this work, we report the synthesis, characterization and application of a new kind of magnetic/luminescent multifunctional nanocomposites (Scheme 1). The nanocomposites were synthesized by using EDC/NHS coupling chemistry to covalently link multiple superparamagnetic Fe_3O_4 NPs stabilized with carboxylic groups of citric acid and individual silica-coated and surface aminolated $NaYF_4$: Yb,Er UCNPs. The resultant

nanocomposites display active functional groups (–NH_2 on the surface of silica-coated UCNPs and –COOH on the iron oxide NPs) on their surface, which enable easy bioconjugation with biomolecules in biomedical applications. They exhibited both good superparamagnetic and excellent up-conversion green photoluminescent properties, which are desired for applications such as magnetic separation and guiding as well as cell imaging. The as-prepared Fe_3O_4/$NaYF_4$: Yb,Er magnetic/luminescent nanocomposites were conjugated with transferrin, which can recognize HeLa cells, and successfully employed for fluorescent imaging of HeLa cells using NIR light to excite them (Scheme 2).

2. Materials and methods

2.1 Materials

All utilized chemical reagents in the experiment such as rare-earth oxide (RE_2O_3), sodium fluoride (NaF), oleic acid ($C_{17}H_{33}COOH$), PEG 4000, tetraethyl orthosilicate (TEOS), 3-aminopropyltrimethoxysilane (APTES), ferric trichloride ($FeCl_3$), ferrous chloride ($FeCl_2$), citric acid ($C_6H_8O_7$) were of analytical grade and used without further purification (purchased from National Medicines Corporation Ltd. of China). *N*-Ethyl-*N*′-[3-(dimethylamino)propyl]carbodiimide hydrochloride (EDC) and *N*-hydroxysuccinimide (NHS) were obtained from Acros (USA). HeLa cells were supplied by China Medical University. Triple-distilled water was used throughout the experiments.

2.2 Synthesis and surface modification of Fe_3O_4 NPs

Monodisperse Fe_3O_4 magnetic NPs were prepared by slightly modifying a reported chemical co-precipitation method.[32] Briefly, 5 mL of a mixture of $FeCl_3$ and $FeCl_2$ with a molar ratio of 2 : 1 was added together with 10 g of PEG 4000 under stirring, followed by adjusting the pH value to 9.5 with ammonia. The resultant solution was kept at 35 °C for 30 min under N_2 protection. The as-prepared Fe_3O_4 precipitations were separated by using a magnet, washed with water until the pH value reached 7.0, then dried at 50 °C for 24 h to get the Fe_3O_4 nanoparticles. In order to allow the magnetic NPs to present carboxyl groups on the surface, citric acid was used to treat the obtained Fe_3O_4 powder, as reported.[17] Briefly, Fe_3O_4 powders were re-suspended in 0.5 M citric acid under ultrasonic (5 mg mL^{-1} Fe_3O_4) under stirring for 4 h. Then the solution was precipitated with acetone and centrifuged at 9000 rpm, and finally dried at 50 °C.

2.3 Synthesis and modification of rare-earth doped $NaYF_4$ UC NPs

A solvothermal approach described previously[33] was used to prepare $NaYF_4$ UCNPs by using rare-earth stearate $(C_{17}H_{35}COO)_3RE$ as the precursor and oleic acid as the stabilizing agent. Briefly, 15 mL of ethanol, 10 mL of water and 5 mL of oleic acid were first mixed together to form a solution, to which 0.9577 g of rare-earth stearate and 0.2100 g of NaF were added under stirring. After about 10 min, the mixture was placed into a 50 mL autoclave, sealed and solvothermally treated at 150 °C for 24 h. After the autoclave was cooled to room temperature, the products were separated by centrifugation, washed with ethanol three times and finally dried at 60 °C for 8 h.

The Stober method was applied to form firstly a silica shell on the as-prepared $NaYF_4$ UCNPs and functionalize the silica-coated UCNPs with amino groups. In a typical experiment, 20 mg $NaYF_4$ NPs were dispersed in 70 mL of ethanol and then sonicated at room temperature for 40 min. Then, a solution of 5 mL of 15% $NH_3 \cdot H_2O$ was added to the mixture, followed by the dropwise addition of 20 μL of TEOS and 200 μL of APTES. Subsequently, the resulting NPs were collected after centrifuging and washing, and dried at 60 °C.

2.4 Synthesis of $Fe_3O_4/NaYF_4$ composite nanoparticles by EDC/NHS coupling

Typically, amino-functionalized 0.0084 g of $NaYF_4$ UCNPs were added to a 20 mL dispersion of carboxyl-functionalized Fe_3O_4 NPs (0.1 mg mL^{-1}) (Scheme 1). The reaction mixture was then briefly ultrasonicated to form a homogenous solution, to which 1 mL of NHS and EDC (both of 0.1 mg mL^{-1}) were added quickly, followed by stirring for 2 h. The $Fe_3O_4/NaYF_4$ nanocomposite products were magnetically separated. The nonmagnetic particles were removed by washing with distilled water and ethanol. The separated products were dried at 60 °C for 8 h.

2.5 Conjugation of transferrin with $Fe_3O_4/NaYF_4$ nanocomposites

In order to test the applications of $Fe_3O_4/NaYF_4$ nanocomposites in immuno-labeling and fluorescent imaging of cancer cells, the nanocomposites were conjugated with a protein called transferrin. Transferrin is known to specifically interact with a transferring receptor that is overexpressed on the HeLa cells. Therefore, the transferring-conjugated nanocomposites will specifically recognize and bind HeLa cells, enabling immunolabeling and fluorescent imaging of HeLa cells by the nanocomposites. The conjugation of transferrin with $Fe_3O_4/NaYF_4$ nanocomposites was completed through the reaction between carboxylic and amino groups under activation of NHS and EDC (Scheme 2). Typically, a solution of 1 mL of $Fe_3O_4/NaYF_4$ nanocomposites (2 mg mL^{-1}) was mixed with 100 μL of 4mgmL^{-1} transferrin, 100 μL of 0.1 mg mL^{-1} NHS and 50 μL of 0.1 mg mL^{-1} EDC, and incubated for 2.0 h at 37 °C in a reciprocating oscillator. Next, the solution was separated by centrifuging, washed with PBS for twice, and resuspended in 400 μL of PBS, stored at 4 °C for further use.

2.6 Biolabeling and imaging of HeLa cells with $Fe_3O_4/NaYF_4$ nanocomposites

The HeLa cells were cultured on glass chamber slides in RPMI 1640 media containing 10% fetal bovine serum and 1% penicillin/streptomycin overnight in a culture box. The cells were washed with PBS for 4 times, blocked in PBS containing 1% BSA for 20 min at 4 °C and then incubated with transferrin conjugated $Fe_3O_4/NaYF_4$ nanocomposites at 37 °C for 1.0 h. In a control experiment, the nanocomposites without conjugation with transferrin were allowed to interact with HeLa cells directly by the aforementioned method. The cells were washed with PBS for four times, and then imaged on an inverted fluorescent microscope (Leica DMIL) equipped with a Nikon digital camera. A 980 nm laser was used to excite the samples during imaging. If the cells are associated with the nanocomposites, the UCNPs will emit green fluorescence in response to the laser irradiation.

3. Results

3.1 Morphology and nanostructure of the nanocomposites

The morphology and size of the as-prepared products were characterized by a JEM-2100HR transmission electron microscope (TEM, JEOL Ltd., Japan), using an accelerating voltage of 200 kV. Fig. 1 shows the TEM images of Fe_3O_4 NPs, $NaYF_4$ UCNPs, $NaYF_4@SiO_2$ NPs and $Fe_3O_4/NaYF_4$ nanocomposites. Fe_3O_4 NPs dispersed in water are about 9 nm in diameter (Fig. 1a). The $NaYF_4$ UCNPs are nearly spherical and fairly well dispersed with an average size of about 45 nm (Fig. 1b). Fig. 1c clearly shows that the particles have a core–shell structure after coating $NaYF_4$ UCNPs with a silica layer and confirms the successful coating of silica around $NaYF_4$ UCNPs. The thickness of the silica shell is approximately 7–10 nm and can be further tuned by adjusting the amount of TEOS and the reaction time. Fig. 1d represents the image of the as-prepared $Fe_3O_4/NaYF_4$ nanocomposites, indicating that carboxyl group-functionalized Fe_3O_4 NPs are combined with and assembled on the surface of amino-modified $NaYF_4$ UCNPs due to the EDC/NHS coupling (Scheme 1). The particle

size of the $Fe_3O_4/NaYF_4$ nanocomposites is about 100–150 nm (Fig. 1d). Conglomeration of $NaYF_4$ UCNPs might occur during the amino modification and could be improved by dispersion with sonication.

In order to investigate the structure and composition of the nanocomposites, XRD and EDS were employed to analyze the products. Powder XRD measurements were performed at room temperature (pXRD, PW3040/60 X'Pert Pro MDP, Holland Panalytical B. V.) by using Cu-Kα (1.5418 Å) radiation. First, crystalline structures of $NaYF_4$ and magnetic iron oxide NPs prepared by modified coprecipitation were characterized by XRD. All of the diffraction peaks of the $NaYF_4$ NPs shown in Fig. 2(a) match well with those for hexagonal β-phase $NaYF_4$ listed in the XRD standard card (No. 00-028-1192), and in Fig. 2(b) the XRD pattern is also in good agreement with the standard pattern of a crystalline cubic structure of Fe_3O_4 (JCPDS No. 01-075-0449). Finally, the pattern shown in Fig. 2(c) illustrates the XRD pattern of $Fe_3O_4/NaYF_4$ nanocomposites, suggesting that the powder was a mixture of hexagonal β-phase $NaYF_4$ and Fe_3O_4 NPs. Furthermore, the diffraction peaks from $NaYF_4$ UCNPs are more dominant than those from Fe_3O_4 NPs, because the nanocomposites are made of smaller Fe_3O_4 NPs assembled around larger individual $NaYF_4$ UCNPs and have a higher percentage of $NaYF_4$ UCNPs (Fig. 1d). Along with TEM results, the XRD data further confirm the successful formation of $Fe_3O_4/NaYF_4$ nanocomposites through EDC/NHS coupling (Scheme 1). It is known that among the two crystalline structure of $NaYF_4$ only hexagonal β-phase can emit strong up-conversion fluorescence, so it is expected that the synthesized nanocomposites should possess excellent optical properties.

An energy dispersed X-ray spectrum (EDS) of the $Fe_3O_4/NaYF_4$ nanocomposites (Fig. 3) shows very strong peaks of Y, F, and relatively strong peaks of Yb, Na, which indicates the existence of $NaYF_4$ in the nanocomposites. The high intensities of these peaks in the EDS spectrum suggest that the prepared nanocomposites will possess efficient up-conversion fluorescence. The presence of peaks for other elements such as Si, C and O in the EDS spectrum confirms the formation of the SiO_2 layer, proving the successful amino modification of the nanocomposites *via* the typical Stober method. In addition to these elements, the spectrum also includes the peaks from Fe, verifying that $Fe_3O_4/NaYF_4$: Yb,Er magnetic-fluorescent nanocompo-sites were successfully prepared. As described below, the successful synthesis of the nanocomposites was further proved by magnetic hysteresis loop and fluorescence images taken with and without a magnet under 980 nm excitation.

3.2 Magnetic and fluorescent properties of the nanocomposites

Fig. 4 shows the hysteresis loops of Fe_3O_4 nanoparticles and $Fe_3O_4/NaYF_4$ nanocomposites, which were measured on a vibrating sample magnetometer (VSM 7407, LakeShore, USA). The saturation magnetization of citric-acid-modified Fe_3O_4 NPs prepared by a facile homogenous precipitation method was 58 emu g^{-1} (Fig. 4a). The value was decreased to 20.3 emu g^{-1} after the NPs were modified with –COOH groups (Fig. 4b). It is known that the saturation magnetization of Fe_3O_4 NPs is closely related to their particle size. During the modification process, citric acid was successfully bound to the surface of Fe_3O_4 through hydrogen bonds, electrostatic attraction and covalent bonds, acting as a stabilizer to prevent the NPs' aggregation. Therefore, after surface modification smaller and more monodispersed Fe_3O_4 NPs were obtained, which leads to the reduction of saturation magnetization. After the formation of $Fe_3O_4/NaYF_4$: Yb,Er magnetic/fluorescent nanocomposites, the saturation magnetization was significantly decreased to 2.85 emu g^{-1} (Fig. 4c). This phenomenon was mainly caused by the presence of high proportion of $NaYF_4$: Yb,Er in the composite NPs, according to the result of EDS analysis shown in Fig. 3. Fortunately, the magnetism of as-synthesized $Fe_3O_4/NaYF_4$: Yb,Er nanocomposites fulfils the requirements for bioseparation and enrichment. In addition, Fig. 4c shows that the

coercivity of the nanocomposites is very low and close to zero, indicating that the nanocomposites have good superparamagnetism. Such good superparamagnetism will make sure that the nanocomposites can be redispersed rapidly as soon as the external magnetic field is removed, which is highly desired for their applications in nanomedicine.

The above characterizations suggest that the nanocomposites made of $NaYF_4$ and Fe_3O_4 NPs should possess both excellent up-conversion fluorescent and superparamagnetic properties. To further confirm these properties, 10 mg of the powders were dispersed in 20 mL of distilled water by ultrasonic for 10 min to form a homogeneous solution, which was further characterized by photoluminescence spectroscopy. As can be seen from Fig. 5, the $Fe_3O_4/NaYF_4$ nanocomposite solution showed a typical luminescence spectrum of $NaYF_4$ NPs at the excitation of 980 nm. The three peaks at 520 nm, 540 nm and 654 nm in the spectrum can be assigned to the $^2H_{11/2} \rightarrow {}^4I_{15/2}$, $^4S_{3/2} \rightarrow {}^4I_{15/2}$ and $^4F_{9/2} \rightarrow {}^4I_{15/2}$ transition, respectively. The luminescence can also be demonstrated by the photos taken by a digital camera with and without an external magnetic field in Fig. 6. Fig. 6(a) shows that the synthesized $Fe_3O_4/NaYF_4$ nanocomposites are dispersed uniformly in water before applying a magnet, can be well separated from the bulk solution phase when a magnet is applied from one side of the cuvette, and then can be readily re-dispersed in water after magnetic separation for 10 min and removing the magnet. Fig. 6(b) shows the corresponding luminescence photos of the solutions in (a), confirming the up-conversion photoluminescence upon irradiation by a NIR light (980 nm). From these results it can be concluded that the as-prepared nanocomposites exhibit superparamagnetism that can be exploited in the detection and enrichment of biomolecules and targeted delivery of drug, as well as NIR-responsive visible light emission that can be used for fluorescent imaging of cells and tissues. It should be noted that the up-conversion luminescence, that is, the emission of visible light (*e.g.*, green light) in response to a NIR light (*e.g.*, 980 nm), is highly desired in bioimaging because it is known that NIR light can penetrate cells and tissues while not damaging them.

3.3 Infrared spectroscopy

Fig. 7 shows infrared spectroscopic characterization of $NaYF_4$, Fe_3O_4 and $Fe_3O_4/NaYF_4$ nanocomposites, which were obtained by a Perkin Elmer Spectrum One spectrometer. As shown in Fig. 7(b), the infrared spectrum of Fe_3O_4 has an obvious absorption peak at 591 cm^{-1}, which is the characteristic peak of Fe–O bond. It also has two other peaks at 1629 and 1397 cm^{-1} assignable to the stretching vibration of carboxyl salt, which indicates that the citric acid has been successfully bound to the surface of the Fe_3O_4 NPs. The peak at 3138 cm^{-1} might result from the stretching vibration of O–H bond in water. In Fig. 7c the peak at 582 cm^{-1} corresponds to the Fe–O bond and the peaks at 1638 and 1559 cm^{-1} are attributed to the deformation vibration of C–H. All of these results suggest that $NaYF_4$ and Fe_3O_4 were conjugated together by EDC/NHS coupling after reaction (Scheme 1). Additionally, peaks at 1087 and 3380 cm^{-1} in Fig. 7(c) also indicate that after conjugation the amino groups still exist on the surface of the composite NPs. These results indicate the presence of amino and carboxyl groups on the nanocomposites' surface which can be used to conjugate the nanocomposites with other biomolecules for labeling biological samples.

3.4 Bio-labeling and imaging of HeLa cells using nanocomposites

As described above, the conjugation of $NaYF_4$ with Fe_3O_4 NPs was achieved through the EDC/NHS coupling reaction between amino and carboxyl groups (Scheme 1). Typically, $NaYF_4$ and Fe_3O_4 NPs were separately functionalized with amino-terminated silane and citric acid, respectively, and then mixed at room temperature for further conjugation. After reaction, the obtained nanocomposites still possess amino and carboxyl groups on the surface, which can be conjugated with biomolecules to make the nanocomposites useful as a

fluorescent probe in the field of biomedicine (Scheme 2). Here, we used the prepared Fe_3O_4/$NaYF_4$ nanocomposites as a probe for the biolabelling of HeLa cells by using transferrin as a linker that can recognize the receptors overexpressed on HeLa cells.[34] First, the nanocomposites were linked with transferrin under activation of NHS and EDC (Scheme 2). After reaction for 4 h, the nanocomposite–trasferrin conjugates were incubated with HeLa cells for 1 h. Finally, the cells were washed with PBS for several times and subjected to fluorescence imaging under excitation by an NIR light.

Fig. 8(a) shows the bright-field, fluorescence and overlays imaging of the HeLa cells that have been incubated with the nanocomposite-labeled transferrin. According to Fig. 8(a), after incubated with nanocomposites, the cell surface exhibits strong green up-conversion fluorescence under 980 nm excitation, implying that the nanocomposite-labeled transferrin is still active and can recognize the receptors on the HeLa cells. Namely, after incubation with HeLa cells, the nanocomposites were transported onto the cells due to the transferrin–transferrin receptor interaction on the cell surface. In contrast, in a control experiment where cells were incubated with Fe_3O_4/$NaYF_4$ nanocomposites without conjugation with transferrin, the cells were imaged under 980 nm excitation after the same incubation process and their surfaces could not emit any green fluorescence under 980 nm excitation (Fig. 8b). These results show very good specific recognition between transferrin and transferrin-receptor on the cell surface when transferrin-conjugated nanocomposites are used as imaging probes. As shown in Fig. 8(c), the HeLa cells without being incubated with any NPs do not show any fluorescence, which is in agreement with the report that the use of NIR light excitation can avoid the auto-fluorescence of biological samples,[33] and further verifies the advantage of using our NIR-responsive nanocomposites for fluorescent imaging of biological samples.

To study the toxicity of the nanocomposites, the incubation was prolonged to 6 h during the biolabelling shown in Fig. 9(b). Compared with Fig. 9(a), prolonged incubation just caused a broader coverage of nanocomposites on the cell surface, while the cells in Fig. 9(b) did not show any obvious damage. The low toxicity of the nanocomposites may arise from the fact that the synthesized Fe_3O_4 nanoparticles were modified with PEG 4000 which could reduce the toxicity and enhance particle stability and biocompatibility.[35,36]

4. Discussion

4.1 Conjugation of Fe_3O_4 and $NaYF_4$ nanoparticles

The principle of the conjugation of Fe_3O_4 and $NaYF_4$ NPs through EDC/NHS coupling chemistry used in our work is schematically illustrated in Scheme 1. Just as described in the Materials and Methods section, during the reaction, Fe_3O_4 and $NaYF_4$ NPs were first modified with carboxyl and amino groups on the surface, respectively. Next, Fe_3O_4 and $NaYF_4$ NPs can be conjugated covalently under the activation of NHS and EDC through the reaction between carboxylic and amino groups (Scheme 1). Finally, multifunctional nanocomposites were obtained. In the control experiment, the $NaYF_4$ NPs without amino group modification were used instead of amino functionalized $NaYF_4$. After the same procedure as described in section 2.4, Fe_3O_4 and $NaYF_4$ NPs did not react to combine during the experiment. Hence, we can conclude that the conjugation of Fe_3O_4 and $NaYF_4$ NPs was induced by carboxylic and amino groups on their surface.

So far, very few reports used covalent binding to integrate the magnetic and fluorescent nanoparticles in a nanocomposite.[8,17] In particular, there has been no report on the covalent bonding of magnetic NPs and fluorescent UCNP core. The chemical conjugation of the magnetic NPs and fluorescent UCNPs in the nanocomposites can enhance the stability of the nanocomposites. Such stability will make it possible to achieve the simultaneous fluorescent

imaging and magnetic guiding in biomedicine. If the magnetic NPs and fluorescent core are detached from each other during bioimaging or bioseparation application, the simultaneous fluorescent imaging and magnetic manipulation by a single nanocomposites will be impossible.

4.2 Biolabeling and imaging of HeLa cells with $Fe_3O_4/NaYF_4$ nanocomposites

The biolabeling of HeLa cells was completed through the reaction between transferrin conjugated with nanocomposites and transferrin receptor on the cancer cell surface (Scheme 2). The as-prepared nanocomposites were already functionalized with carboxyl and amino groups due to the presence of –COOH functionalized iron oxide NPs assembled around the $–NH_2$ functionalized UCNP core in the nanocomposites and could be directly used without any further modification. During the experiment, the nanocomposites were first conjugated with transferrin, which can recognize receptors on the HeLa cells, under the activation of NHS and EDC to become a bioprobe that can recognize and fluorescently label the HeLa cells (Scheme 2). When the nanocomposites labeled with transferrin are incubated with HeLa cells, the transferrin will specifically recognize and bind transferrin-receptor on the cell surface, so the cell surface will be capped with the probe which emits green up-conversion fluorescence under 980 nm excitation. As a result, the cancer cells can be fluorescently labeled by our nanocomposites and imaged under the irradiation of an NIR light.

The $Fe_3O_4/NaYF_4$ nanocomposites made of magnetic Fe_3O_4 and fluorescent $NaYF_4$ integrate the advantages of both magnetic and fluorescent nanoparticles. Our work on the biolabeling of HeLa cells has demonstrated the biocompatibility and applicability of the $Fe_3O_4/NaYF_4$ nanocomposites in fluorescent biodetection. Other than the application in fluorescent detection, the nanocomposites can also be employed in magnetic bioseparation due to the presence of the magnetic nanoparticles. Magnetic bioseparation is a very effective tool for the separation of biomolecules into bound and unbound fractions and can overcome the disadvantages of the conventional separation methods, resulting in improved detection sensitivity and shortened measurement time.[17,14] Therefore, the fluorescent, magnetic and water-soluble properties of the $Fe_3O_4/NaYF_4$ nanocomposites would allow them to find a variety of applications such as biolabeling, bioseparation, and immunoassays. More studies on the magnetic and fluorescent nanocomposites will enable further applications in bioanalytical chemistry, clinical medicine, biology and pharmacology.

5. Conclusion

Monodisperse $Fe_3O_4/NaYF_4$ nanocomposites with good up-conversion luminescent and superparamagnetic properties were prepared *via* the covalent coupling reaction between carboxyl groups on the surface of Fe_3O_4 and amino groups on the surface of silica-coated $NaYF_4$ UCNPs. The nanocomposites can be pictured as the assembly of multiple Fe_3O_4 superparamagnetic NPs around individual $NaYF_4$ UCNPs. They bear functional carboxyl and amino groups on the surface which can be used to form conjugates with biomolecules for biolabeling. The nanocomposites were successfully used as probes for biolabeling and imaging of HeLa cells. The nanocomposites will serve as a new multifunctional probe for simultaneous fluorescent detection and magnetic separation of biomolecules and cells. The presence of the UCNPs components in the nanocomposites will allow the imaging of the biological samples under an NIR light with minimum auto-fluorescence from the biological samples.

Acknowledgments

We are grateful for the support from the National Science Foundation of China (Grant Nos 20875011, 20675012) and the Education Committee of Liaoning Province of China as well as the support from Northeastern University for PhD students. C.-B. M. would like to acknowledge the financial support from US National Science Foundation, National Institutes of Health, Department of Defense Breast Cancer Research Program and Oklahoma Center for the Advancement of Science and Technology.

References

1. Wang X, Wang LY, He XW, Zhang YK, Chen LX. Talanta. 2009; 78:327–332. [PubMed: 19203590]
2. Zhang Y, Kohler N, Zhang MQ. Biomaterials. 2002; 23:1553–1661. [PubMed: 11922461]
3. Shen LF, Laibinis PE, Hatton AT. Langmuir. 1999; 15:447–453.
4. Chen ZL, Sun Y, Huang P, Yang XX, Zhou XP. Nanoscale Res. Lett. 2009; 4:400–408. [PubMed: 20596490]
5. Palma CD, Colombo M, Allevi R, Nebuloni M, Ronchi S, Rizzi G, Tosoni A, Trabucchi E. Small. 2009; 5(22):2555–2564. [PubMed: 19634132]
6. Corr SA, Rakovich YP, Gun'ko YK. Nanoscale Res. Lett. 2008; 3:87–104.
7. Gao JH, Gu HW, Xu B. Acc. Chem. Res. 2009; 42:1097–1107. [PubMed: 19476332]
8. Zhang Y, Wang SN, Ma S, Guan JJ, Li D, Zhang XD, Zhang ZD. J. Biomed. Mater. Res., Part A. 2008; 85a:840–846.
9. Yu L, Yin YD, Mayers BT, Xia YN. Nano Lett. 2002; 2:183–186.
10. Zhang BB, Cheng J, Gong XQ, Dong XQ, Liu XH, Ma GP, Chang J. J. Colloid Interface Sci. 2008; 322:485–490. [PubMed: 18430431]
11. Wang DS, He JB, Rosenzweig N, Rosenzweig Z. Nano Lett. 2004; 4(3):409–413.
12. Tian ZQ, Zhang ZL, Gao JH, Huang BH, Xie HY, Xie M, Abrun HD, Pang DW. Chem. Commun. 2009:4025–4027.
13. Gao JH, Zhang Wei. Huang PB, Zhang B, Zhang XX, Xu B. J. Am. Chem. Soc. 2008; 130:3710–3711. [PubMed: 18314984]
14. Hong X, Li J, Wang MJ, Xu JJ, Guo W, Li JH, Bai YB, Li TJ. Chem. Mater. 2004; 16:4022–4027.
15. Romlan DG, May SJ, Zheng JG, Allan JE, Wessels BW, Lauhon LJ. Nano Lett. 2006; 6:50–54. [PubMed: 16402786]
16. Kim H, Achermann M, Balet LP, Hollingsworth JA, Klimov VI. J. Am. Chem. Soc. 2005; 127:544–546. [PubMed: 15643877]
17. Sun P, Zhang HY, Liu C, Fang J, Wang M, Chen J, Zhang JP, Mao CB, Xu SK. Langmuir. 2010; 26:1278–1284. [PubMed: 19775134]
18. Zhang MF, Shi SJ, Meng JX, Wang XQ, Fan H, Zhu YC, Wang XY, Qian YT. J. Phys. Chem. C. 2008; 112:2825–2830.
19. Son A, Dosev D, Nichkova M, Ma ZY, Kennedy IM, Scow KM, Hristova KR. Anal. Biochem. 2007; 370:186–194. [PubMed: 17869209]
20. Ma ZY, Dosev D, Nichkova M, Gee SJ, Hammock BD, Kennedy IM. J. Mater. Chem. 2009; 19:4695–4700. [PubMed: 20357905]
21. Setua S, Menon D, Asok A, Nair S, Koyakutty M. Biomaterials. 2010; 31:714–729. [PubMed: 19822364]
22. Zhang YX, Pan SS, Teng XM, Luo YY, Li GH. J. Phys. Chem. C. 2008; 112:9623–9626.
23. Auzel F. Chem. Rev. 2004; 104:139–173. [PubMed: 14719973]
24. Wang X, Li YD. Chem. Commun. 2007:2901–2910.
25. Zhao JW, Sun YJ, Kong XG, Tian LJ, Wang Y, Tu LP, Zhao JL, Zhang H. J. Phys. Chem. B. 2008; 112:15666–15672. [PubMed: 19367869]
26. Heer S, Kömpe K, Güdel HU, Haase M. Adv. Mater. 2004; 16:2102–2105.
27. Ehlert O, Thomann R, Darbandi M, Nann T. ACS Nano. 2008; 2:120–124. [PubMed: 19206555]
28. Li ZQ, Zhang Y, Jiang S. Adv. Mater. 2008; 20:4765–4769.

29. Wang M, Mi CC, Zhang YX, Liu JL, Li F, Mao CB, Xu SK. J. Phys. Chem. C. 2009; 113(44): 19021–19027.
30. Wang M, Hou W, Mi CC, Wang WX, Xu ZR, Teng HH, Mao CB, Xu SK. Anal. Chem. 2009; 81(21):8783–8789. [PubMed: 19807113]
31. Lu HC, Yi GS, Zhao SY, Chen DP, Guo LH, Cheng J. J. Mater. Chem. 2004; 14:1336–1341.
32. Xie J, Xu CJ, Kohler N, Hou YL, Sun SH. Adv. Mater. 2007; 19:3163–3166.
33. Wang M, Mi CC, Wang WX, Liu CH, Wu YF, Xu ZR, Mao CB, Xu SK. ACS Nano. 2009; 3:1580–158. [PubMed: 19476317]
34. Wu J, Ye ZH, Wang GL, Yuan JL. Talanta. 2007; 72:1693–1697. [PubMed: 19071818]
35. Kamimura M, Miyamoto D, Saito Y, Soga K, Nagasaki Y. Langmuir. 2008; 24:8864–8870. [PubMed: 18652424]
36. Xu LX, Kim MJ, Kim KD, Choa YH, Kim HT. Colloids Surf., A. 2009; 350:8–12.

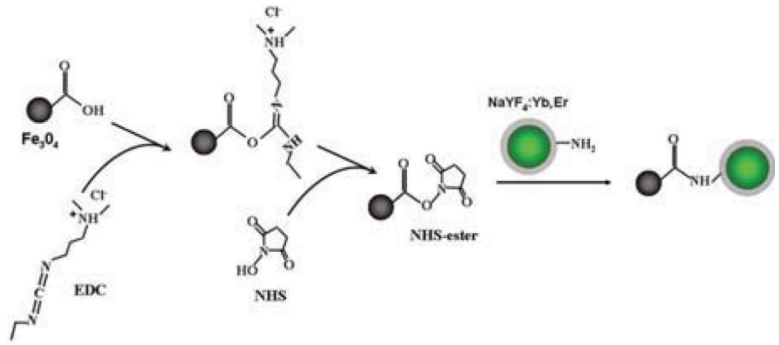

Scheme 1.
Schematic illustration of the formation of $Fe_3O_4/NaYF_4$ nanocomposites through EDC/NHS coupling chemistry.

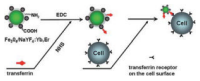

Scheme 2.
Diagram for biolabelling of HeLa cells with $Fe_3O_4/NaYF_4$ nanocomposites using EDC/NHS coupling chemistry.

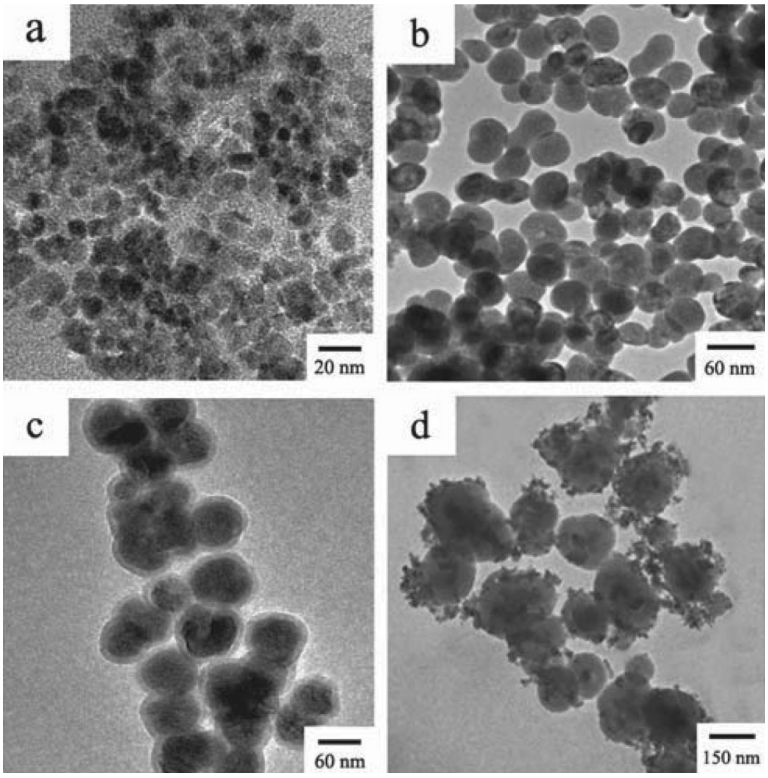

Fig. 1.
TEM images of Fe_3O_4 nanoparticles (a), $NaYF_4$ nanoparticles (b), $NaYF_4@SiO_2$ nanoparticles (c) and $Fe_3O_4/NaYF_4$ nanocomposites (d).

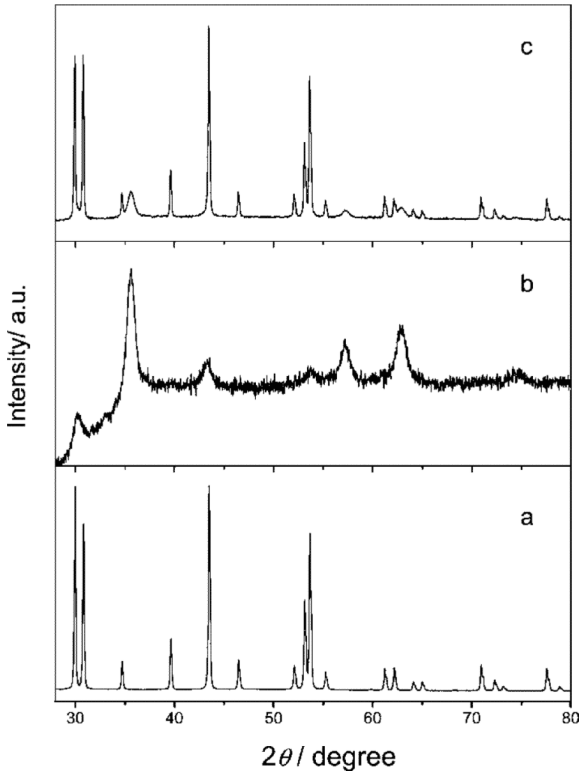

Fig. 2.
XRD patterns of $NaYF_4$ nanoparticles (a), Fe_3O_4 nanoparticles (b) and $Fe_3O_4/NaYF_4$ nanocomposites (c).

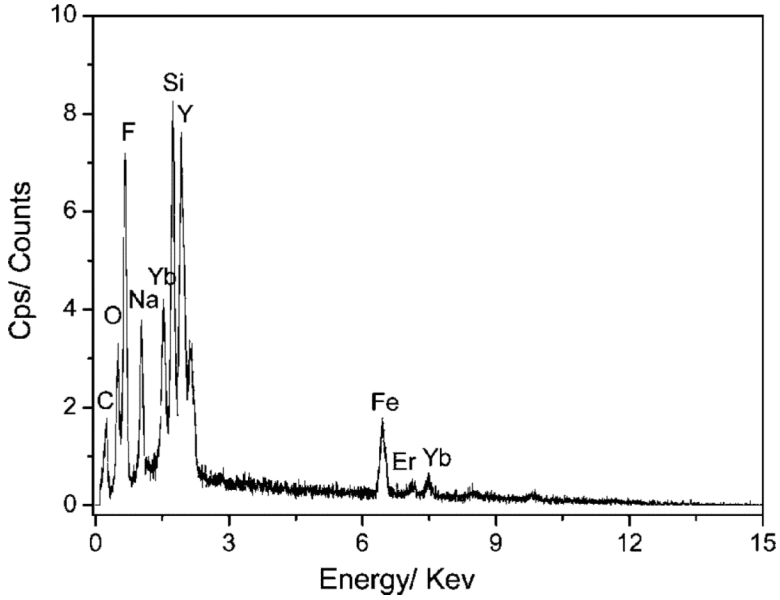

Fig. 3.
The EDS analysis of $Fe_3O_4/NaYF_4$ nanocomposites.

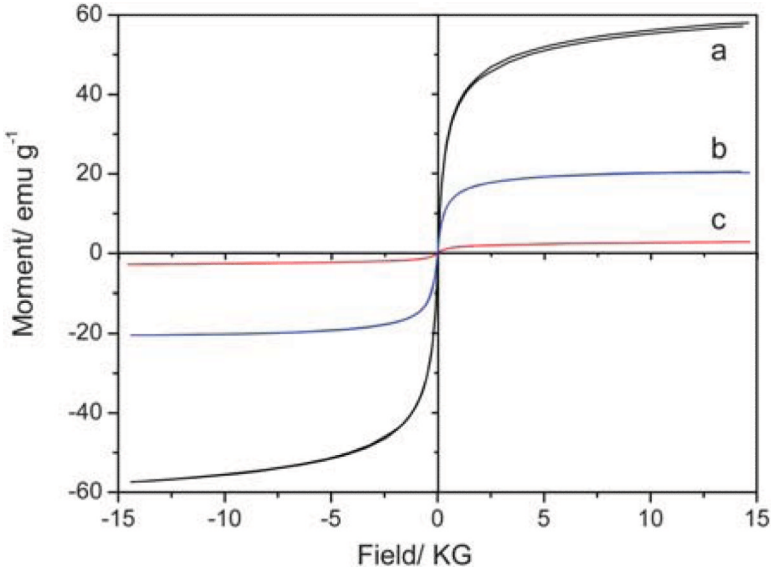

Fig. 4.

Hysteresis loops for the Fe_3O_4 nanoparticles (a), Fe_3O_4–COOH nanoparticles (b), and Fe_3O_4/$NaYF_4$ nanocomposites (c).

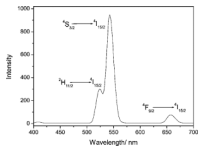

Fig. 5.
The typical luminescence spectrum of the $Fe_3O_4/NaYF_4$ composites when they are excited by a NIR light (980 nm).

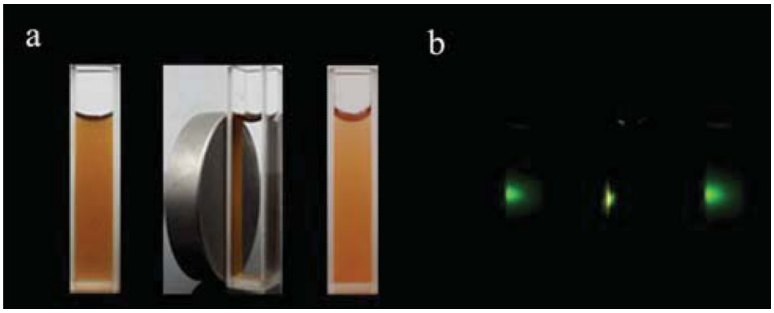

Fig. 6.

Bright field (a) and dark field under 980 nm excitation (b) photographs of aqueous solution of the as-synthesized $Fe_3O_4/NaYF_4$ nanocomposites before applying a magnetic field (left), in the presence of a magnet (middle) and redispersed after removing the magenet (right).

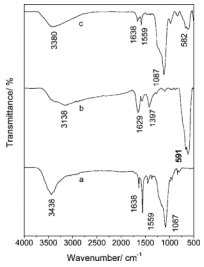

Fig. 7.
The IR spectra of $NaYF_4$ nanoparticles (a), Fe_3O_4 nanoparticles (b) and $Fe_3O_4/NaYF_4$ nanocomposites (c).

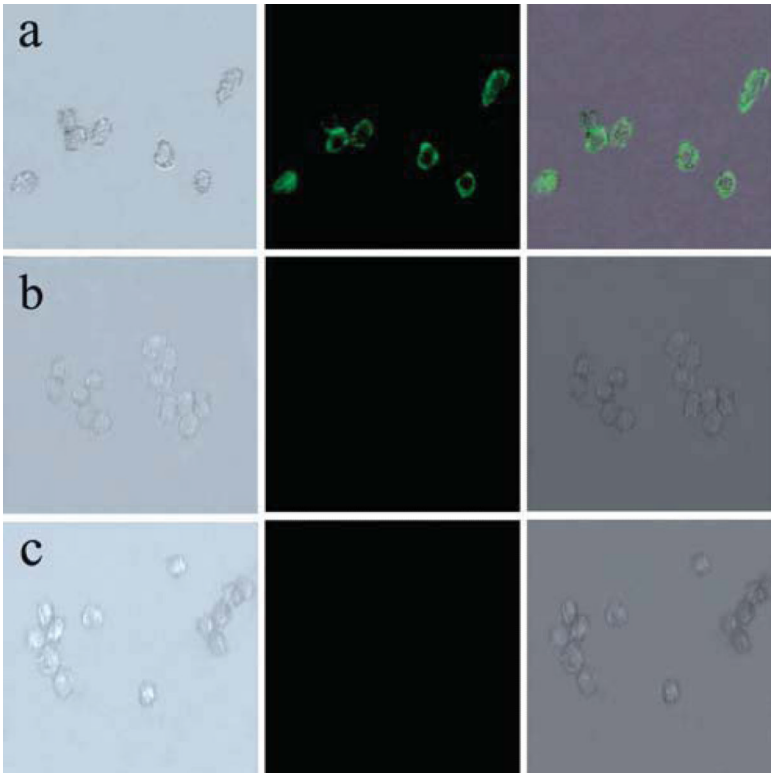

Fig. 8.

Images of live HeLa cells after being incubated with $Fe_3O_4/NaYF_4$ nanocomposites biolabeled with transferrin (a), after being incubated with $Fe_3O_4/NaYF_4$ nanocomposites without transferrin conjugated (b), and without incubating with any nanoparticles (c). In the three panels, the left rows are images in bright field, the central rows represent fluorescent images in dark field and the right rows are the overlays of the left and central rows.

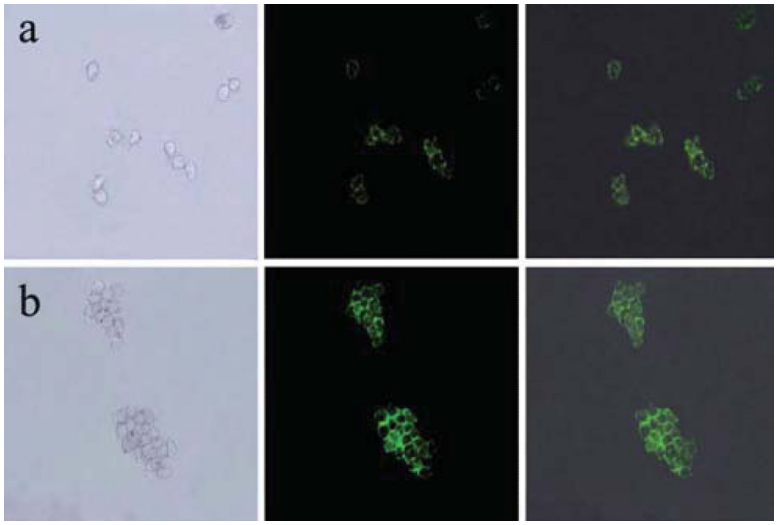

Fig. 9.

Images of live HeLa cells after being incubated with $Fe_3O_4/NaYF_4$ nanocomposites biolabeled with transferrin incubated (a) for 1 h and (b) for 6 h. In the three panels, the left rows are images in bright field, the central rows represent fluorescent images in dark field and the right rows are the overlays of the left and central rows.